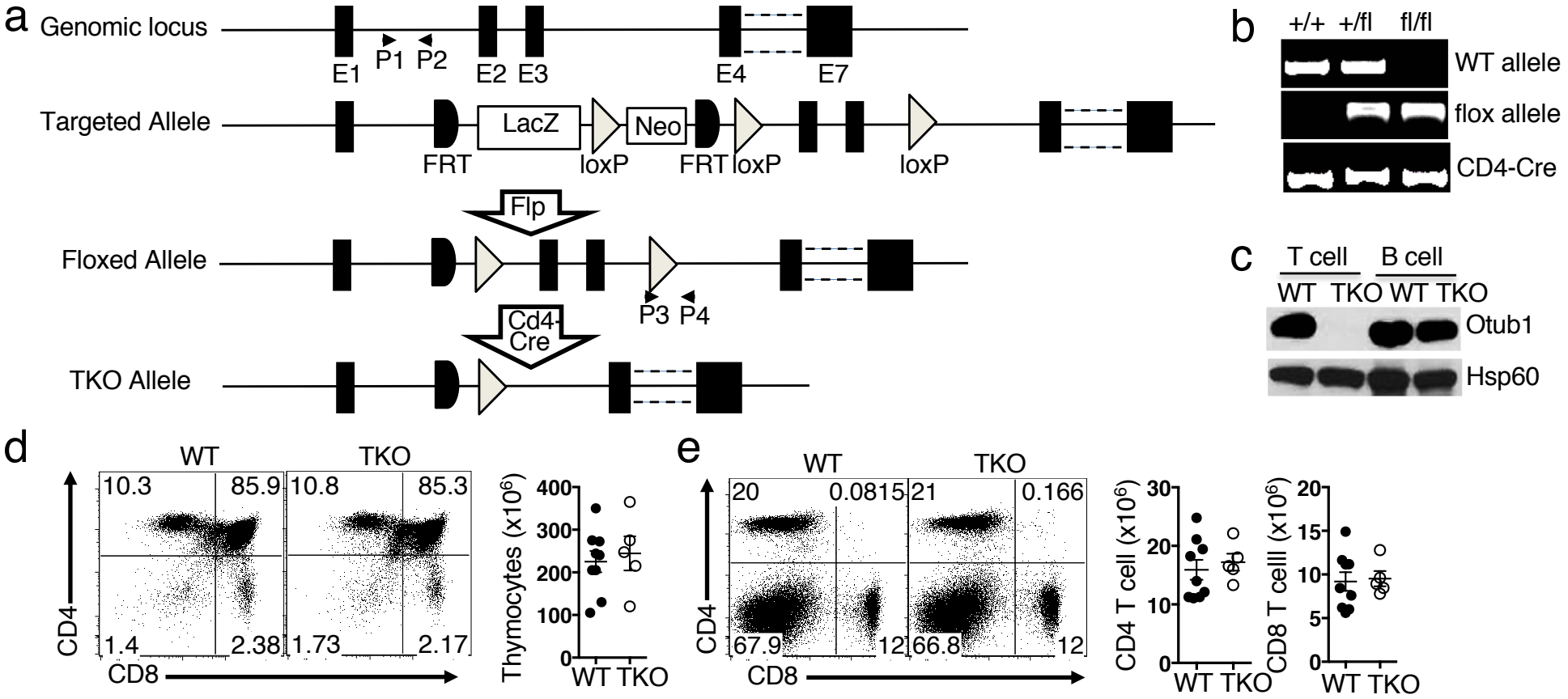


**Supplementary Fig. 1. Otub1 deficiency does not influence the frequency of thymocyte and peripheral T cell populations. a,** Schematic picture of *Otub1* gene targeting using an FRT-LoxP vector. Targeted mice were crossed with FLP deleter (Rosa26-FLPe) mice to generate *Otub1*-floxed mice, which were further crossed with *Cd4*-Cre mice to generate T cell-conditional KO (TKO) mice. **b,** Genotyping PCR analysis of floxed and control mice using P1/P2 primer pair for WT allele and P3/P4 primer pair for flox allele. **c,** Immunoblot analysis of Otub1 using sorted T and B cells from WT or *Otub1*-TKO mice. **d,** Flow cytometric analysis of thymocytes from WT and *Otub1*-TKO mice (6 wk old), showing the percentage of $CD4^{-}CD8^{-}$ double negative, $CD4^{+}CD8^{+}$ double positive, and $CD4^{+}$ and $CD8^{+}$ single positive populations. A summary graph of total thymocyte cell number is shown. **e,** Flow cytometric analysis of frequency of CD4 and CD8 T cells in the splenocytes of WT and *Otub1*-TKO mice.

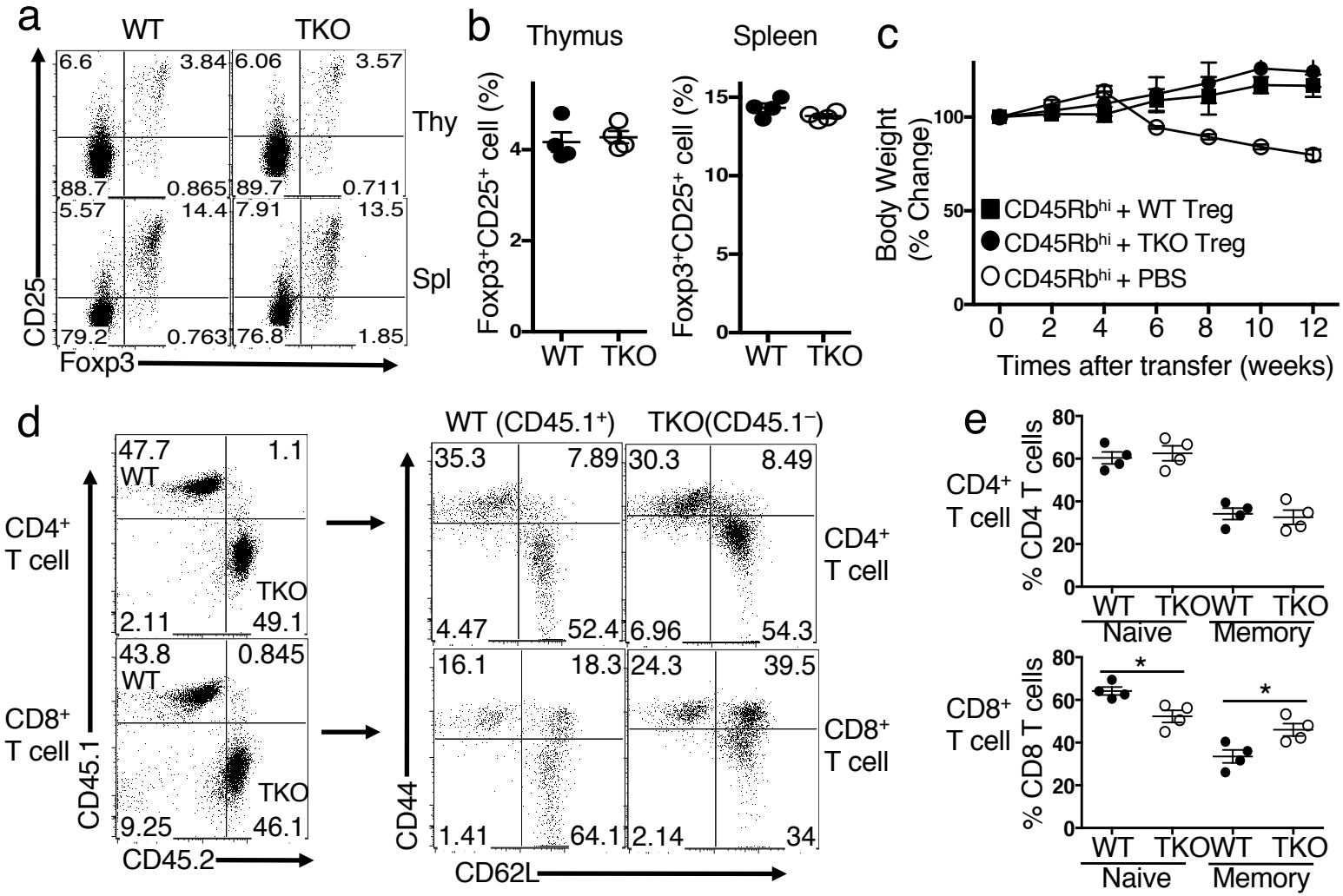


**Supplementary Fig. 2. Otub1 is dispensable for Treg cell generation and function. a,b,** Flow cytometric analysis of the frequency of Treg cells (Foxp3$^{+}$CD25$^{+}$) among CD4$^{+}$ T cells in the thymus and spleen of age- and sex-matched WT and *Otub1*-TKO mice (6-8 weeks), presented as a representative plot (**a**) and summary graph based on multiple mice (**b**, each circle represents an individual mouse). **c,** Body weight loss of 6-week-old *Rag1*-TKO mice following adoptive transfer with WT naïve CD45RB$^{hi}$ CD4 T cells together with either PBS (CD45RB$^{hi}$+PBS) or sorted Treg cells derived from 6-week-old WT mice (CD45RB$^{hi}$+WT Treg) or Otub1-TKO mice (CD45RB$^{hi}$+TKO Treg). **d,** Bone marrow cells (2 x 10$^{6}$) from *Otub1*-TKO (CD45.1$^{-}$CD45.2$^{+}$) and WT B6.SJL (CD45.1$^{+}$CD45.2$^{-}$) mice were mixed in 1:1 ratio and adoptively transferred into γ-irradiated *Rag1*-TKO mice. After 6 weeks, recipient mice were sacrificed for flow cytometric analyses of CD4 and CD8 T cells derived from WT and Otub1-TKO bone marrows (left) and the naïve and memory populations based on CD44 and CD62L markers (naïve: CD44$^{lo}$CD62L$^{hi}$; memory: CD44$^{hi}$CD62L$^{lo}$) (right). **e,** Summary graphs of the naïve and memory T cell data from **d** based on four recipients of each group. *$P<0.05$(two-tailed unpaired t test).

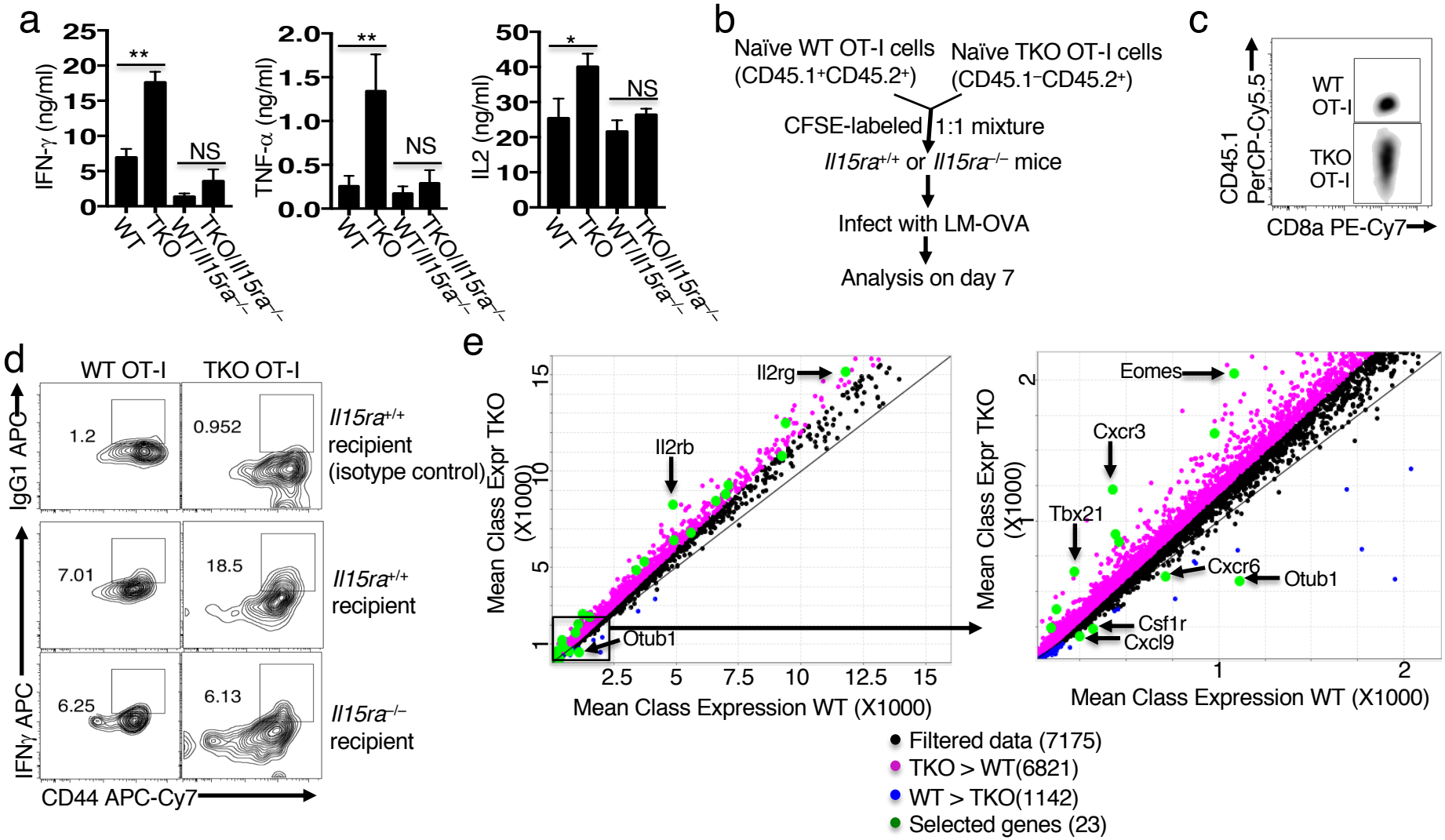


**Supplementary Fig. 3. IL-15 primes CD8 T cells for activation under the control of Otub1. a,** ELISA of naïve CD8 T cells derived from WT, *Otub1*-TKO, WT/*Il15ra*$^{-/-}$, and *Otub1*-TKO/*Il15ra*$^{-/-}$ mice, in vitro stimulated with anti-CD3 plus anti-CD28 for 66 h. **b,** Schematic of mixed T cell adoptive transfer and listeria infection. *Il15ra*$^{+/+}$ or *Il15ra*$^{-/-}$ mice were adoptively transferred with CFSE-labeled WT OT-I or *Otub1*-TKO OT-I naïve CD8 T cells mixed in 1:1 ratio (5 x $10^6$ cells each) and infected with ovalbumin-expressing recombinant Listeria monocytogenes (LM-OVA, 2 x $10^4$). Transferred OT-I cells were analyzed 7 days later. **c,d,** Flow cytometric analysis of total population (**c**) or IFNγ-producing effector frequency of WT and *Otub1*-TKO OT-I cells isolated from the LM-OVA-infected recipient mice shown in **b**, stimulated *in vitro* with OVA257-274 for 6 h (**d**). **e**, Scatterplot of significantly upregulated (pink, 6821genes) and downregulated (blue, 1142 genes) genes in *Otub1*-TKO OT-I T cells relative to WT OT-I T cells. Some of the genes presented in the heatmap shown in Fig. 2g are indicated in green color. RNA sequencing was performed with RNA isolated from untreated naïve WT or *Otub1*-TKO OT-I CD8 T cells. NS, non-significant; *P<0.05; **P<0.01, two-tailed student's t-test.

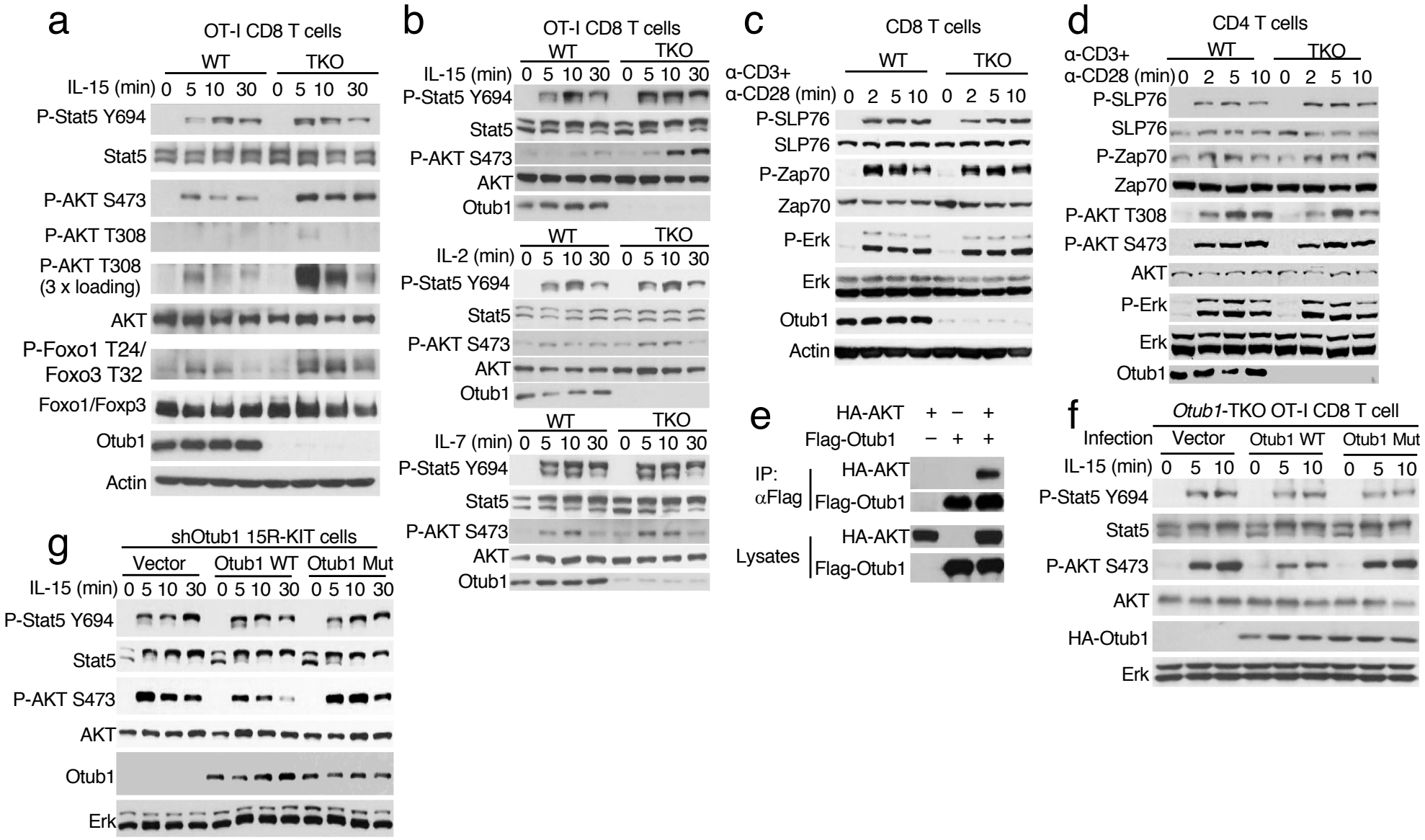


**Supplementary Fig. 4. Otub1 negatively regulates AKT activation in CD8 T cells. a-c,** Immunoblot analysis of the indicated phosphorylated (P-) and total proteins in naïve OT-I CD8 T cells (**a**,**b**), naïve CD8 T cells (**c**), or naïve CD4 T cells (**d**) stimulated with the indicated inducers. A panel of P-AKT T308 with 3 times more loading materials (3 x loading) was included in **a** to visualize the weak AKT T308 phosphorylation stimulated by IL-15. **e,** Co-IP analysis of Otub1-AKT interaction in HEK293 cells transiently transfected with expression vectors encoding the indicated proteins. **f**,**g**, Immunoblot analysis of the indicated phosphorylated (P-) and total proteins in IL-15-stimulated Otub1-deficient OT-I CD8 T cells (**f**) or Otub1-knockdown 15R-KIT T cells (**g**) infected with an empty retroviral vector or vectors encoding Otub1 wildtype (WT) or an inactive mutant (Mut, D88A/C91S).

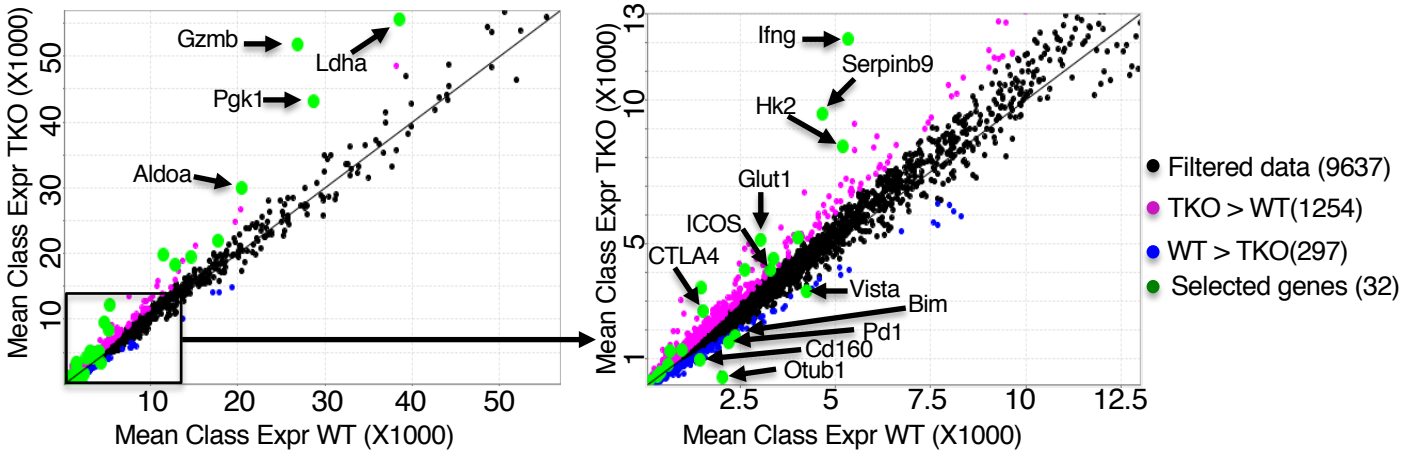


**Supplementary Fig. 5. Otub1 controls gene expression in CD8 T cells.** Scatterplot of significantly upregulated (pink, 1254) and downregulated (blue, 297) genes in Otub1-TKO OT-I T cells relative to WT OT-I T cells stimulated with anti-CD3 plus anti-CD28 for 24 h and analyzed by RNA sequencing. Some of the genes presented in the heatmap of Fig. 6a are indicated in green color.

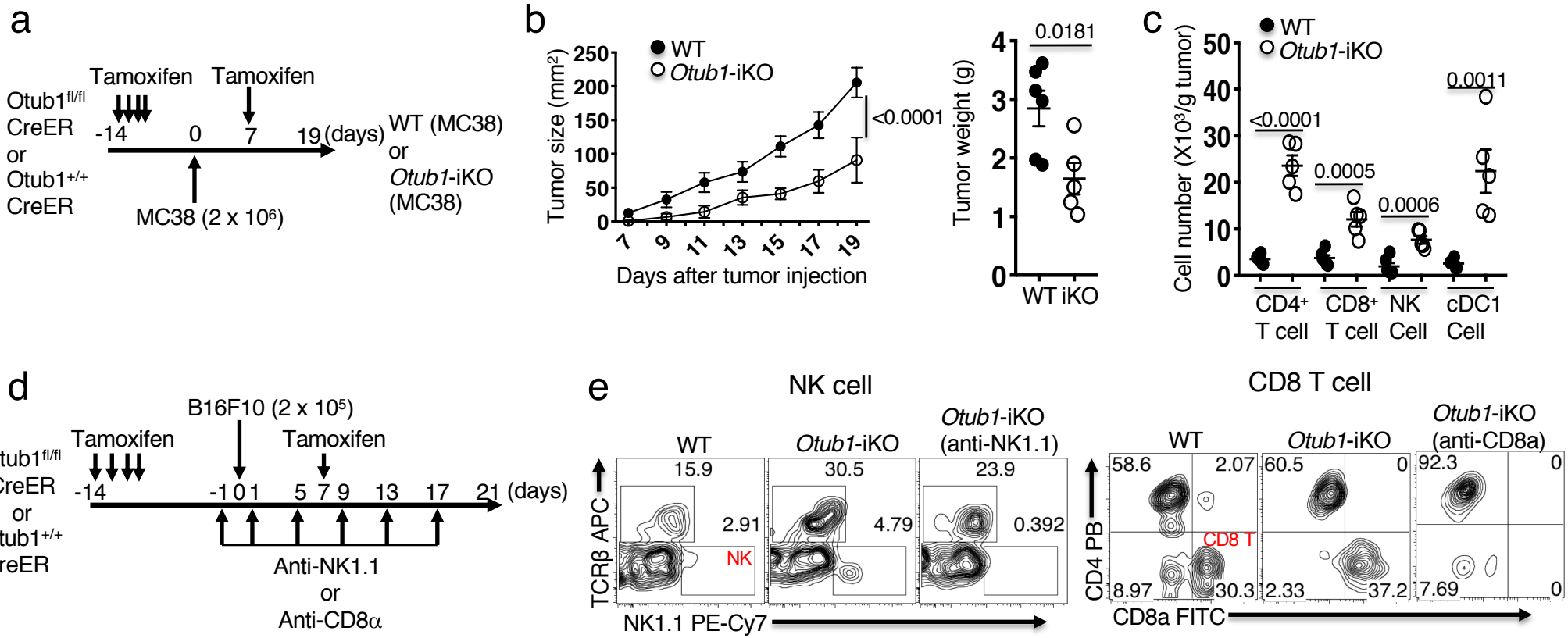


**Supplementary Fig. 6. Otub1 deletion promotes antitumor immunity via CD8 T cells and NK cells. a**, Schematic of experimental procedure, in which the indicated mice were injected with tamoxifen daily for 4 consecutive times starting from day 14 before tumor cell inoculation and one more time on day 7 after tumor inoculation for generating WT or *Otub1* induced KO (iKO) MC38-bearing mice. **b**, Tumor burden of WT and *Otub1*-iKO mice, presented as tumor grow curve (left) and day 19 tumor weight (right). **c**, Summary graph of flow cytometric analysis of tumor-infiltrating immune cells in WT and *Otub1*-iKO mice. **d,e**, Schematic of experimental procedure, in which the indicated mice were injected with tamoxifen daily for 4 consecutive times starting from day 14 before tumor cell inoculation and one more time on day 7 after tumor inoculation for generating WT or *Otub1*-iKO B16F10-bearing mice. Some of the tumor-bearing mice were also injected i.p with anti-NK1.1 and anti-CD8a for depletion of NK cells and CD8 T cells, respectively. (**e**) Flow cytometric analysis of NK cells and CD8 T cells showing the efficiency of antibody-mediated depletion. P values are determined by two-way ANOVA with Bonferroni's post-test (**b**) or two-tailed student's t-test (**c**).

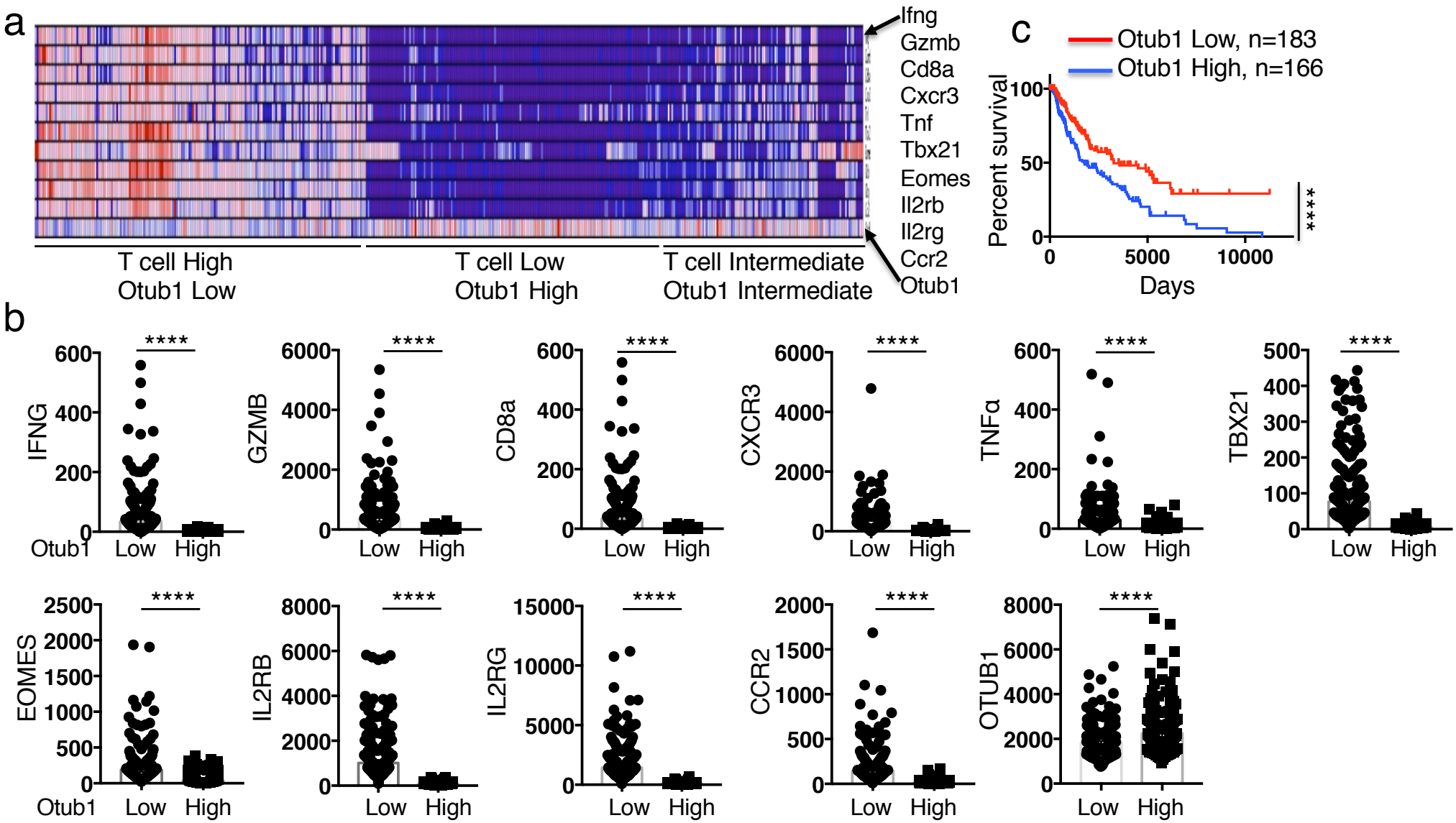


**Supplementary Fig. 7. Otub1 expression level is inversely associated with patient survival and effector T cell signature gene expression in skin cutaneous melanoma. a**, Heatmap illustrating the expression of major CD8 effector T cell signature genes (rows) across the 458 skin cutaneous melanoma patients (columns). The color scale of the heatmap indicates relative gene expression. **b**, mRNA level of CD8 T cell signature genes in Otub1 low and high group. ****P<0.0001, two-tailed student's t-test. **c**, Kaplan-Meier plot comparing survival for the two broad clusters of patients identified in hierarchical clustering analysis. (p<0.0001, Log-Rank test).

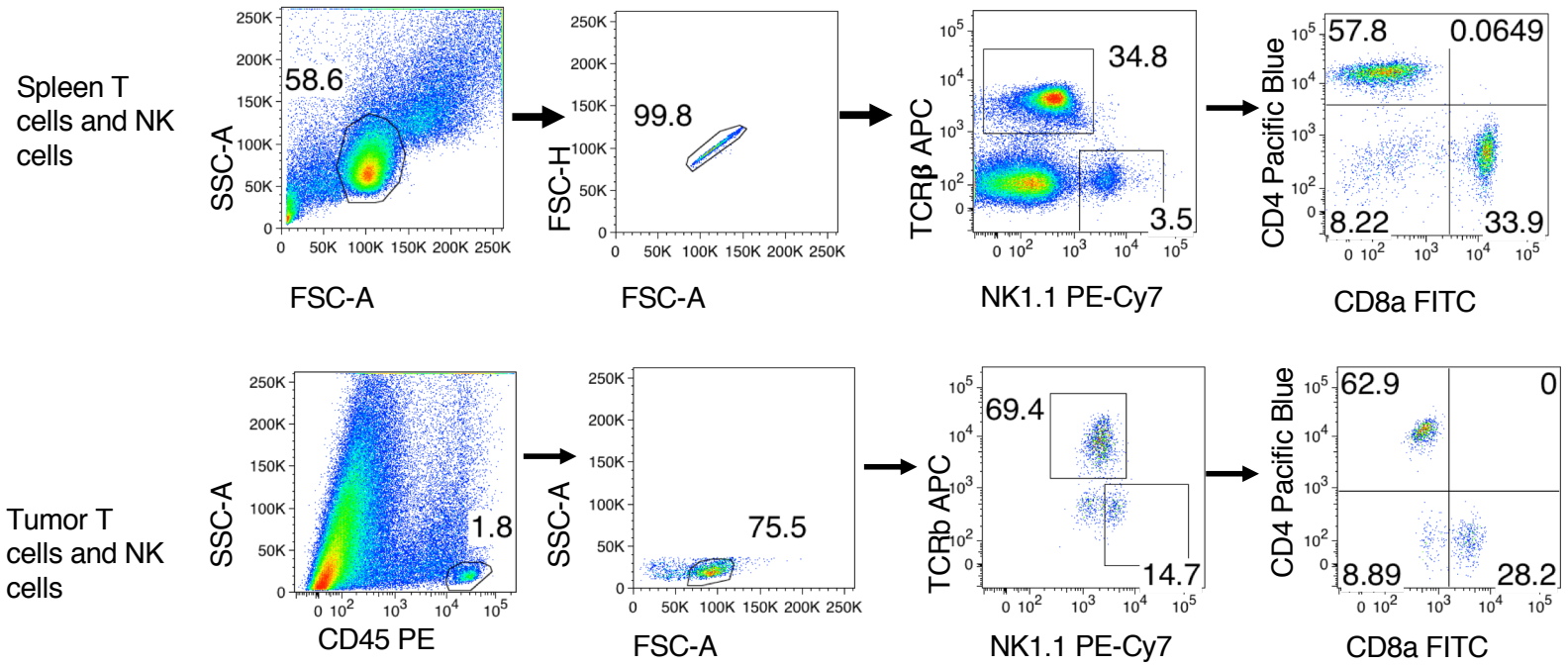


**Supplementary Fig. 8.** Live immune cell populations were gated on the FSC-A and SSC-A, and single cells were gated basing on FSC-A and FAS-H. The subpopulations of the indicated immune cells were gated basing on specific surface markers as indicated in the individual panels.

figure 3b

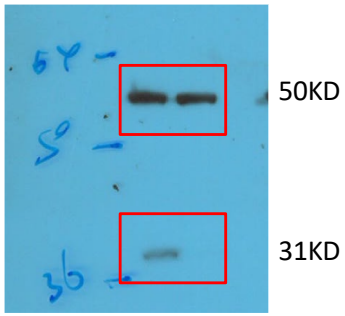


**Supplementary Figure 9. Full scans of blots for figures 3b.**

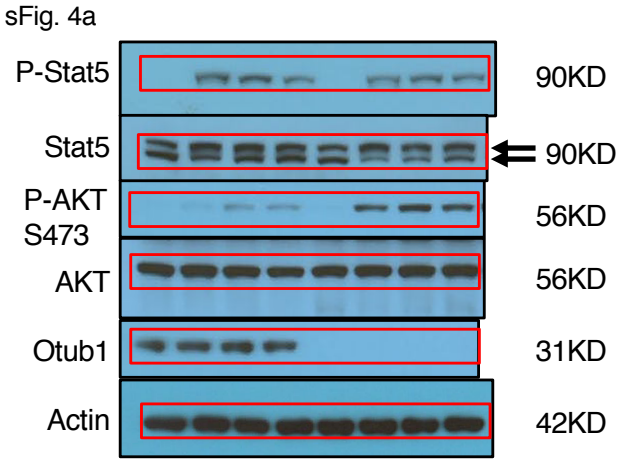


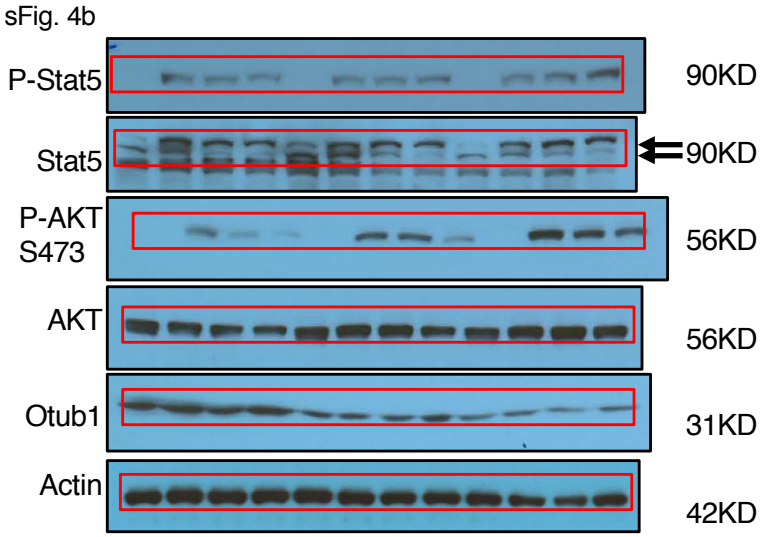


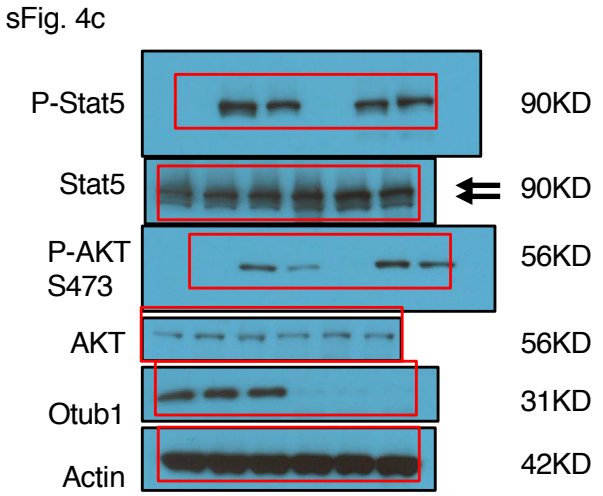


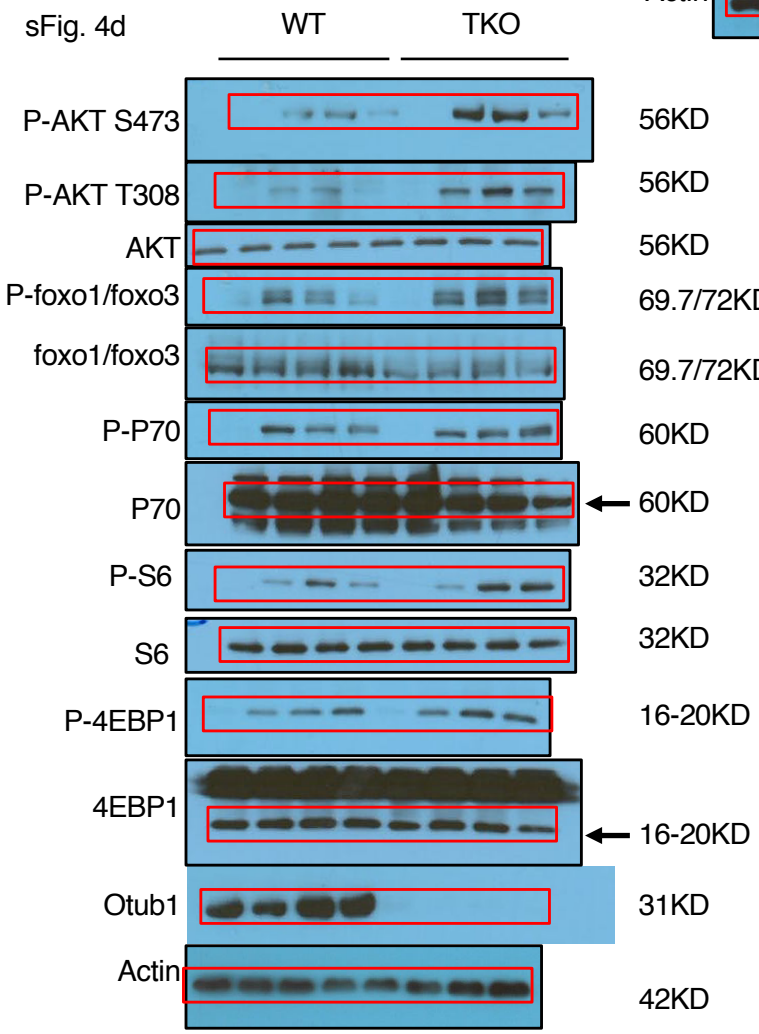


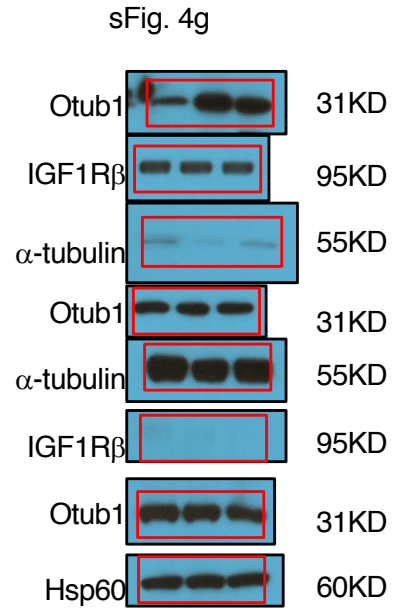


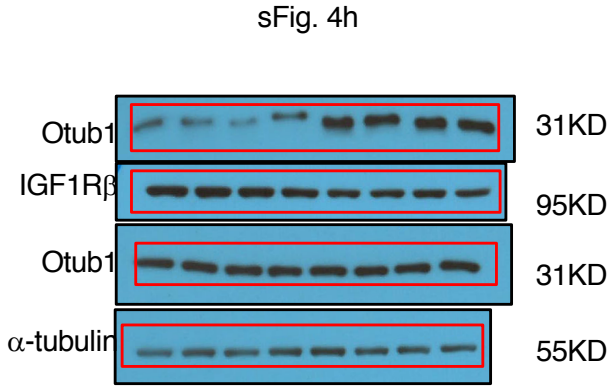


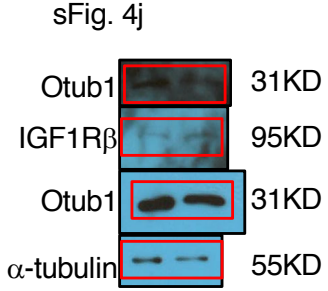


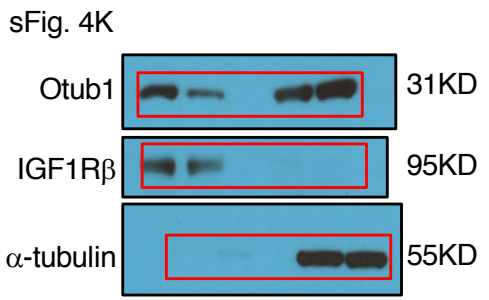


**Supplementary Figure 10. Full scans of blots for figures 4a-4d and 4g-4k.**

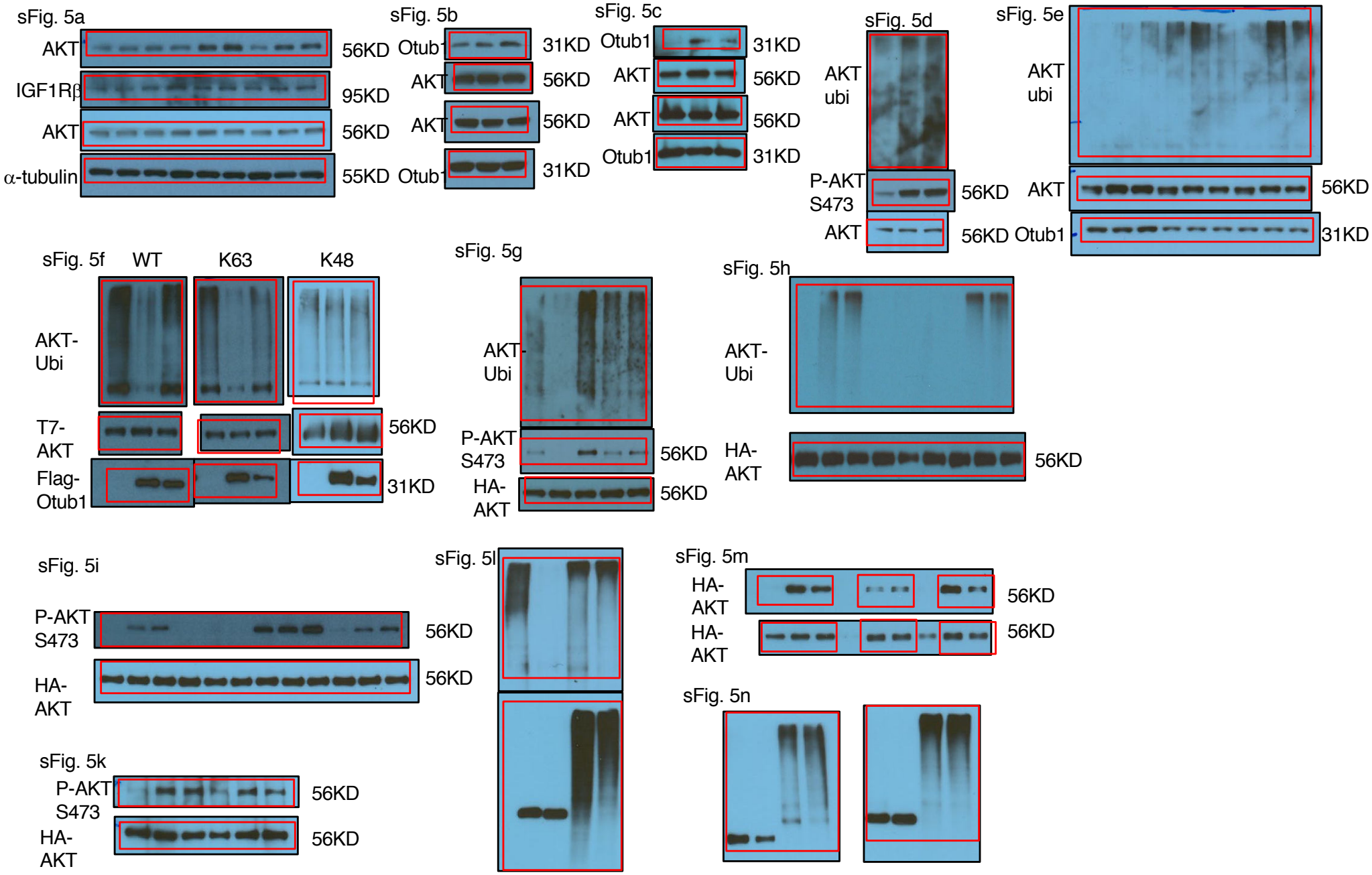


**Supplementary Figure 11. Full scans of blots for figures 5a-5i and 5k-5m.**

figure 6b

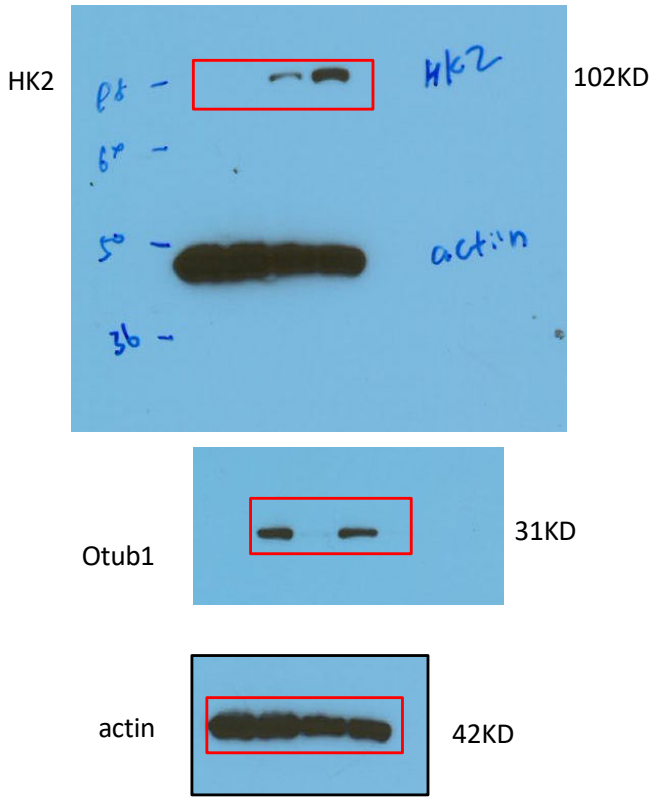


**Supplementary Figure 12. Full scans of blots for figures 6b.**